

Quasiparticle band structure calculation of monolayer, bilayer, and bulk MoS₂

Tawinan Cheiwchanchamnangij and Walter R. L. Lambrecht

Department of Physics, Case Western Reserve University, Cleveland, Ohio 44106-7079, USA

(Received 25 March 2012; revised manuscript received 14 April 2012; published 2 May 2012)

Quasiparticle self-consistent GW calculations of the band structures and related effective-mass parameters are carried out for bulk, monolayer, and bilayer MoS₂. Including excitonic effects within the Mott-Wannier theory, quantitative agreement is obtained between the A , B excitons, measured by absorption [*Phys. Rev. Lett.* **105**, 136805 (2010)], and the calculated exciton gap energies at K . The A - B splitting arises from the valence-band splitting which in the monolayer is entirely due to spin-orbit coupling and leads to spin-split states, while in the bilayer it is a combined effect of interlayer and spin-orbit coupling.

DOI: [10.1103/PhysRevB.85.205302](https://doi.org/10.1103/PhysRevB.85.205302)

PACS number(s): 73.22.-f, 71.20.Nr, 71.35.-y, 78.55.-m

I. INTRODUCTION

Bulk 2H-MoS₂ is well known to be an indirect gap semiconductor with a 1.29-eV gap.¹ It has a layered structure with van der Waals interaction between the layers. However, this material has gained a lot of interest after it became possible to prepare it in monolayer and few-layer form, by a similar exfoliation technique as applied to graphene.^{2,3} The monolayer MoS₂ has recently been used to build transistors with a very promising mobility.⁴ Moreover, their optical properties are also attractive. A very strong photoluminescence (PL) peak at 1.9 eV is observed in the monolayer and proposed to be a direct transition. Although a lot weaker than PL from the monolayer, bilayer and few-layer films also show the so-called A and B exciton peaks as reported in Ref. 5. Here we report a study of the electronic structure for bulk, monolayer, and bilayer MoS₂ and the excitonic effect which plays an important role in monolayer and bilayer MoS₂, in order to understand their optical properties.

II. COMPUTATIONAL METHODS

The experimental lattice constants have been used, but the atomic positions in the lattice were obtained by minimizing the total energy using the full-potential linearized muffin-tin orbital method⁶ (FP-LMTO) within the local-density approximation^{7,8} (LDA) calculation. The von Barth-Hedin exchange correlation functional is used.⁹ We use the quasiparticle self-consistent GW method¹⁰⁻¹² (QSGW) which has been proven to be very accurate and better than single-shot GW or G_0W_0 in obtaining the band structures.¹⁰ Here G stands for the one-electron Green's function and W for the screened Coulomb interaction and their product defines the quasiparticle self-energy corrections.

In both monolayer and bilayer, the separations between layers from the closest supercell are set to be 19 Å. We have tested that increasing these separations would not affect the band structure. In the LDA calculations k -point meshes of $14 \times 14 \times 7$, $14 \times 14 \times 3$, and $14 \times 14 \times 7$ have been used in monolayer, bilayer, and bulk, respectively. The uniform mesh density along the x , y , and z directions of $25 \times 25 \times 150$ divisions for monolayer, $25 \times 25 \times 198$ divisions for bilayer, and $25 \times 25 \times 98$ divisions for bulk are used for the smooth parts of the potential, charge density, and wave functions. For Mo atoms, a double κ -basis set was used as envelope functions

up to f states in the first κ and up to d states for the second κ . The semicore Mo-4 p states were included as local orbitals. In the case of S atoms, a double κ -basis set was also used but up to d states for the first κ and up to p states for the second. The calculations were converged to the change in total energy less than 10^{-6} Ry. The positions of the atoms were relaxed until the maximum force between atoms less than 1 mRy/au.

The QSGW calculations were started from the LDA calculations. They were performed with an $8 \times 8 \times 2$ k -point mesh for monolayer and bulk, while an $8 \times 8 \times 1$ mesh was used for the bilayer. Floating orbitals were added in the big interstitial sites and between the layers to improve the basis set for high-energy unoccupied states.

The calculations are performed first in the scalar relativistic approximation and spin-orbit coupling (SOC) is then added by re-diagonalizing the double sized Hamiltonian matrices including the GW self-energy correction. Spin-orbit coupling arises mostly from the inner parts of the atom so that this is a good approximation.

III. RESULTS

A. Band structure

As previously reported by Li *et al.*¹³ and also by Lebègue and Eriksson¹⁴ using generalized gradient approximation (GGA) calculations, we also find a transition from an indirect band gap in bulk and bilayer to a direct band gap in the monolayer MoS₂ as shown in Fig. 1. This contrasts the recent G_0W_0 results by Olsen *et al.*¹⁵ who found an indirect gap even in the monolayer. The reason for this discrepancy is not entirely clear. Even at the G_0W_0 level, we find a direct gap in the monolayer, which is 0.2 eV larger than the QSGW result. The difference may result from other technical aspects of the calculations, such as our use of an all-electron method and inclusion of Mo-4 p semicore states as local orbitals in the basis set.

Although both bulk and bilayer MoS₂ have indirect gaps, the former's smallest gap is from Γ to Σ_{\min} where Σ_{\min} is located between the K and Γ points, while the latter's gap is from Γ to K . In the case of monolayer MoS₂ the direct gap is located at the K point. In the bilayer, the conduction-band minimum (CBM) has already shifted from Σ to K but the valence-band maximum (VBM) is still at Γ . From bilayer to monolayer, the VBM shifts from Γ to K . The QSGW results

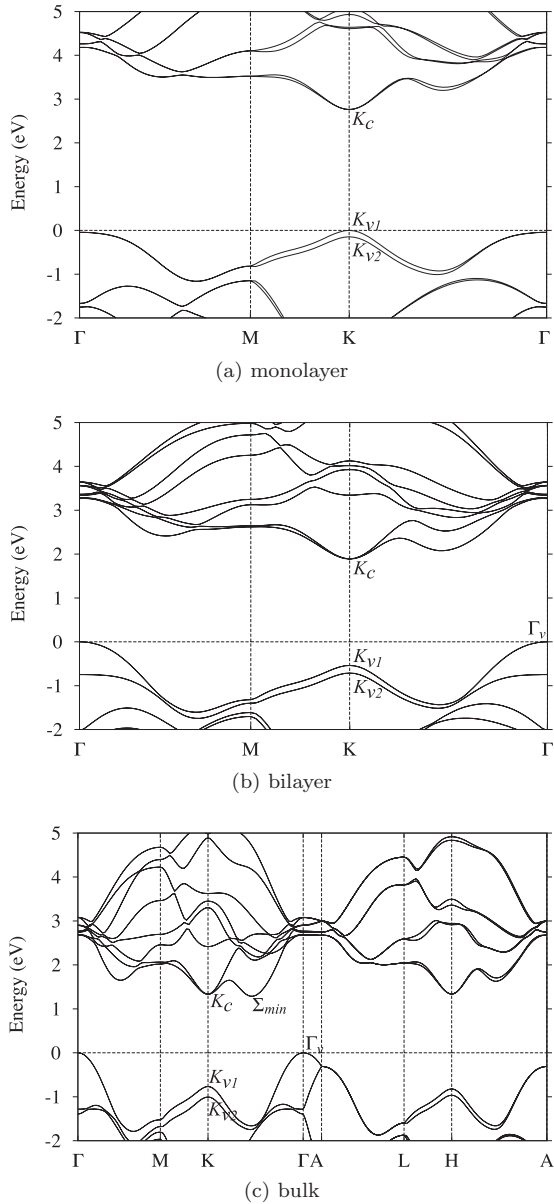


FIG. 1. Band structures of monolayer (a), bilayer (b), and bulk (c) MoS₂ from QSGW calculations.

of the interband transitions near the gap, including the SOC effect, are shown in Table I. The indirect band gap of bulk MoS₂ is in good agreement with the experimental values from optical absorption. Our calculations overestimate the direct gap at *K* by about 0.2–0.3 eV. The calculated transitions in the monolayer and bilayer are overestimated by more than 0.5 eV compared to the optical-absorption measurements.⁵ The large overestimation of these transitions in these systems is due to the large excitonic effect in a two-dimensional system which will be discussed later in this paper. It is important to point out that the splitting of the valence-band maximum of the monolayer at the *K* point is purely because of the spin-orbit effect and the lack of inversion symmetry which has been studied earlier.¹⁷ The same splitting for the bilayer is caused by the combination of the interlayer interaction and the spin-orbit coupling effect. Without spin-orbit coupling the splitting in the bilayer and the

TABLE I. Interband transitions near the gap in monolayer, bilayer, and bulk MoS₂.

Structures	Transitions	Transition energy (eV)	
		Calculated	Experiment ^a
Monolayer	K_{v1} to K_c	2.759	1.90
	K_{v2} to K_c	2.905	2.05
Bilayer	Γ_v to K_c	1.888	1.6
	K_{v1} to K_c	2.427	1.88
	K_{v2} to K_c	2.601	2.05
Bulk	Γ_v to Σ_{min}	1.287	1.29
	K_{v1} to K_c	2.099	1.88
	K_{v2} to K_c	2.337	2.06

^aRef. 16 for bulk direct gap, Ref. 5 for monolayer and bilayer.

bulk are 98 and 188 meV, respectively. In bilayer and bulk the inversion symmetry combined with time reversal implies Kramers degeneracy of the states, so no spin splitting. These splittings of 146 meV in the monolayer and 174 meV in the bilayer agree very well with the energy difference between the *A* and *B* exciton peaks in the absorption spectrum reported in Ref. 5. It is worth noting that the CBM at the *K* point of both monolayer and bilayer MoS₂ also split but with a much smaller (only 4 meV) splitting due to the SOC effect.

B. Estimate of excitonic effects

We use the Mott-Wannier effective-mass theory within the plane. We assume that at the length scale of the exciton Bohr radius, the electron and hole are both confined to $z = 0$ in the plane. As is well known,¹⁸ the Coulomb interaction in the plane is then screened by an effective dielectric constant $\kappa = \sqrt{\varepsilon_{\parallel}\varepsilon_{\perp}}$ with ε_{\parallel} , ε_{\perp} the dielectric tensor components parallel and perpendicular to the *c* axis, respectively. Because the binding energies that result are well above the phonon frequencies, the electronic contribution only is included in the dielectric screening. The latter is obtained directly from our QSGW calculations and shown in Table III. The present values do not include local field effects and are obtained as explained in Ref. 19. We note that they are much smaller than the bulk values. Our values for bulk and monolayer differ somewhat from those given by Molina-Sánchez and Wirtz,²⁰ which are obtained from a different approach, namely by calculating $\partial P/\partial E$ the derivative of the polarization as function of a static electric field within density functional perturbation theory and using Berry-phase theory for the polarization. Both calculations however agree on a strong reduction of the dielectric screening in the monolayer compared to the bulk. We also give the bulk dielectric constants calculated by Reshak and Auluck²¹ for comparison.

In general, both electron and hole may have an anisotropic mass tensor in the plane with longitudinal and transverse components. However, inspecting the various band-edge effective masses and exciton reduced masses in Tables II we can see that both for the direct exciton at *K* and the indirect exciton from $\Gamma \rightarrow K$, the mass tensor is very close to isotropic.

The exciton problem in this case reduces to the well-known isotropic two-dimensional (2D) Coulomb problem with energy

TABLE II. Values of effective masses in unit of electron mass of monolayer and bilayer MoS₂ from various band edge. The subscripts l and t refer to the masses calculated from the longitudinal and transversal direction of the line from Γ point to that point, respectively.

Structures	Points	Effective masses		
		Electron	Hole	Reduced
Monolayer	K_l	0.342	0.455	0.195
	K_t	0.350	0.428	0.193
	Σ_l	0.547	-0.608	5.452
	Σ_t	1.182	3.108	0.856
	Γ_v			0.275 ^a
Bilayer	K_l	0.386	0.459	0.210
	K_t	0.390	0.490	0.217
	Σ_l	0.553	-0.700	2.633
	Σ_t	0.825	7.361	0.742

^aThis value is calculated from the hole effective mass at Γ_v and average value of electron effective mass from both directions at K and is relevant for the indirect gap exciton.

levels

$$E_N = -\frac{E_0}{(N - \frac{1}{2})^2}, \quad \text{for } N = 1, 2, \dots \quad (1)$$

in terms of an effective Bohr radius and Rydberg:

$$a_B = \frac{\hbar^2 \kappa}{\mu e^2}, \quad E_0 = \frac{e^2}{2\kappa a_B}. \quad (2)$$

The ground-state exciton thus has a binding energy of $4E_0$.

Using the values from Tables II and III, the effective Bohr radius is 9.3 Å for monolayer and 13.0 Å for bilayer. This is not large but still large enough relative to the in-plane lattice constant, that the Wannier exciton theory should still be at least approximately applicable. The effective Rydbergs are 0.224 and 0.106 eV for monolayer and bilayer, respectively. These lead to the ground-state binding energy of 0.897 eV for monolayer and 0.424 eV for bilayer. The optical transitions after adding the excitonic effect are reported in Table IV. From this table, we can see that for the monolayer, the gaps from K_{v1} to K_c and K_{v2} to K_c agree very well with the exciton peaks A and B reported in Ref. 5. For the same gaps in the bilayer, the calculation results with excitonic effect overestimate the exciton peaks by 0.12 eV. The indirect exciton gap in the bilayer is now slightly underestimated instead of overestimated.

TABLE III. Values of the dielectric constants of monolayer, bilayer, and bulk MoS₂.

	Direction	Dielectric constant (ϵ)		
		Monolayer	Bilayer	Bulk
Ours	\parallel	2.8	4.2	8.5
	\perp	4.2	6.5	13.5
Ref. 20	\parallel	1.63		7.43
	\perp	7.36		15.40
Ref. 21	\parallel			10
	\perp			16

TABLE IV. Near band-gap optical transitions including the excitonic effect.

Structures	Transitions	Transition energy (eV)		
		Calculated	With exciton	Experiment ^a
Monolayer	K_{v1} to K_c	2.759	1.862	1.90
	K_{v2} to K_c	2.905	2.008	2.05
Bilayer	Γ_v to K_c	1.888	1.341	1.6
	K_{v1} to K_c	2.427	2.003	1.88
	K_{v2} to K_c	2.601	2.177	2.05

^aFrom Ref. 5.

In the case of bulk MoS₂, the exciton binding energy is much smaller than in the monolayer and bilayer, because there is no factor 1/4 in the denominator when compared to the 2D case in Eq. (1) and the dielectric constant is much larger in bulk. Essentially, the masses are similar, the dielectric constants increase by a factor 3 but come in squared in the effective Rydberg, so roughly we expect the exciton binding energy to be about 40 times smaller, or of order 25 meV. In fact, in that case, one needs to use the static dielectric constants. This is compatible with our good agreement (to within 0.1 eV) between QSGW gaps for bulk and experiment without any exciton corrections.

IV. DISCUSSION

While our results suggest that exciton peaks A and B are from the spin-split direct transitions at the point K , Olsen *et al.*¹⁵ explained the same peaks as two distinct strongly bound excitons, one associated with the K point and the other with the minimum in the conduction band at Σ_{\min} . In fact, they find the latter to be the conduction-band minimum but the lowest direct gap is still at K . There is a saddle-point-type extremum in the energy-band differences between the upper valence band and lowest conduction band near the point Σ_{\min} because the valence band also has a minimum near that same point. In the Bethe-Salpeter equation (BSE) approach for excitons, used by them, the electron-hole pairs associated with different k points are allowed to mix but their analysis of their calculated spectrum revealed the lowest exciton peak to be associated with K and the next one with Σ_{\min} . Since in our present calculations the gap is direct and the direct transitions near Σ_{\min} lie sufficiently high in the continuum of the bands, it seems unlikely that electron-hole excitonic effects on this saddle point would be sufficiently strong to pull out a separate localized exciton from the bands. Nonetheless it would be of interest to repeat the BSE calculations with the more accurate QSGW band structure as input. The mixing of excitonic effects at different k points as well as missing polaronic effects could be responsible for the remaining discrepancies of our exciton gaps with experiment. The Wannier exciton theory turns out not be applicable at all to the Σ_{\min} exciton. The larger reduced mass implies a Bohr radius smaller than the in-plane lattice constant and the unusual strongly anisotropic mass, associated with the saddle-point structure, would lead to an unreasonably large binding energy.

V. CONCLUSIONS

Our QSGW calculations show that the transition from indirect to direct gap between bulk and monolayer actually already occurs between bilayer and monolayer, in agreement with experiment.⁵ We find that the splitting of the *A* and *B* excitons is well accounted for by the splittings of the valence bands, which in the monolayer arises purely from spin-orbit coupling. The exciton binding energies however are large for the mono- and bilayer due to the strongly reduced dielectric constants. A Mott-Wannier exciton calculation, although at the limits of its applicability range using our calculated dielectric

constants and effective masses, leads to excellent quantitative agreement between theory and experiment for the *A* and *B* excitons as well as the indirect exciton in the bilayer.

ACKNOWLEDGMENTS

This work was supported by the National Science Foundation under Grant No. DMR-1104595. We thank Jie Shan and Jesse Kinder for useful discussions. This work made use of the High Performance Computing Resource in the Core Facility for Advanced Research Computing at Case Western Reserve University.

-
- ¹Gmelin *Handbook of Inorganic and Organometallic Chemistry*, 8th ed. (Springer-Verlag, Berlin, 1995), Vol. B7.
- ²A. Splendiani, L. Sun, Y. Zhang, T. Li, J. Kim, C. Chim, G. Galli, and F. Wang, *Nano Lett.* **10**, 1271 (2010).
- ³K. S. Novoselov, D. Jiang, F. Schedin, T. J. Booth, V. V. Khotkevich, S. V. Morozov, and A. K. Geim, *Proc. Natl. Acad. Sci. USA* **102**, 10451 (2005).
- ⁴B. Radisavljevic, A. Radenovic, J. Brivio, V. Giacometti, and A. Kis, *Nat. Nanotechnol.* **6**, 147 (2011).
- ⁵K. F. Mak, C. Lee, J. Hone, J. Shan, and T. F. Heinz, *Phys. Rev. Lett.* **105**, 136805 (2010).
- ⁶M. Methfessel, M. van Schilfgaarde, and R. A. Casali, in *Electronic Structure and Physical Properties of Solids. The Use of the LMTO Method*, Lecture Notes in Physics Vol. 535, edited by H. Dreyssé (Springer-Verlag, Berlin, 2000), p. 114.
- ⁷P. Hohenberg and W. Kohn, *Phys. Rev.* **136**, B864 (1964).
- ⁸W. Kohn and L. J. Sham, *Phys. Rev.* **140**, A1133 (1965).
- ⁹U. von Barth and L. Hedin, *J. Phys. C* **5**, 1629 (1972).
- ¹⁰M. van Schilfgaarde, T. Kotani, and S. Faleev, *Phys. Rev. Lett.* **96**, 226402 (2006).
- ¹¹M. van Schilfgaarde, T. Kotani, and S. V. Faleev, *Phys. Rev. B* **74**, 245125 (2006).
- ¹²T. Kotani, M. van Schilfgaarde, and S. V. Faleev, *Phys. Rev. B* **76**, 165106 (2007).
- ¹³T. Li and G. Galli, *J. Phys. Chem. C* **111**, 16192 (2007).
- ¹⁴S. Lebègue and O. Eriksson, *Phys. Rev. B* **79**, 115409 (2009).
- ¹⁵T. Olsen, K. W. Jacobsen, and K. S. Thygesen, e-print arXiv:1107.0600 [cond-mat].
- ¹⁶A. R. Beal and H. P. Hughes, *J. Phys. C* **12**, 881 (1979).
- ¹⁷Z. Y. Zhu, Y. C. Cheng, and U. Schwingenschlögl, *Phys. Rev. B* **84**, 153402 (2011).
- ¹⁸L. D. Landau and E. M. Lifschitz, *Electrodynamics of Continuous Media*, Course of Theoretical Physics Vol. 8 (Butterworth Heinemann, Oxford, 1987).
- ¹⁹M. van Schilfgaarde and M. I. Katsnelson, *Phys. Rev. B* **83**, 081409 (2011).
- ²⁰A. Molina-Sánchez and L. Wirtz, *Phys. Rev. B* **84**, 155413 (2011).
- ²¹A. H. Reshak and S. Auluck, *Phys. Rev. B* **68**, 125101 (2003).